Effect of mitigation on the catastrophic failure of storage tanks

Islem Megdiche [a], William Atherton [a], David Allanson [b], Clare Harris [a],*

[a] Department of Civil Engineering, Liverpool John Moores University, 3 Bayrom St, Liverpool, L3 3AF, UK
[b] Department of Maritime and Mechanical Engineering, Liverpool John Moores University, 3 Bayrom St, Liverpool, L3 3AF, UK

ARTICLE INFO

ABSTRACT

This work investigates the effect of incorporating mitigation techniques on the catastrophic collapse of above-ground storage tanks in terms of dynamic pressures and overtopping fractions using Computational Fluid Dynamics (CFD). Catastrophic Overtopping Alleviation of Storage Tanks (COAST) and Mitigation of Tank Instantaneous Failure (MOTIF) protection measures are implemented. COAST is a deflector fitted to the top of the bund wall that is a structure surrounding a storage tank and MOTIF is a baffle fitted inside the storage tank. An optimisation study has been conducted to select the optimum mitigation technique and the optimum inclination angle of COAST. Subsequently, the effect of incorporating mitigation techniques using different capacities and shapes of bund wall is investigated along with the effect of using various heights of the fluid within the tank. Results show that COAST alone is more effective than combining the two mitigation techniques and the optimum inclination angle giving the lowest dynamic pressures and overtopping fractions is 80°. COAST significantly reduces the overtopping fractions ranging between 93% and 98% for the various capacities investigated. The highest reduction corresponds to a bund wall capacity of 200% of the capacity of the tank. The effect of COAST in reducing the overtopping fractions is more significant for circular shapes than square, rectangular, and triangular walls. Regarding the height of the fluid, COAST is more effective for tall tanks compared to middle and squat tanks.

1. Introduction

Gravity or density flows are generated when a heavier fluid propagates into a lighter one (Huppert and Simpson, 1980; Necker et al., 2002; Cantero et al., 2008). They are frequently encountered in many natural and engineering applications. Some of the various examples encompass snow avalanches, thunder storms, and pyroclastic flows from volcanic eruptions (Simpson, 1997; Cantero et al., 2008; Zgheib et al., 2015). Other examples include oil spills into a river, abrupt gas releases into the atmosphere, and discharge of industrial waste into rivers or sea (Huppert and Simpson, 1980), to name but a few. Gravity flows are characterised by four main phases (Huppert and Simpson, 1980; Simpson, 1997). In the first phase, when the flow is initiated, it keeps accelerating until a maximum velocity is attained and the flow structure changes from vertical to horizontal. This phase is referred to the acceleration phase which is very short, complex, and transitional. In the second phase termed the slumping phase, the flow becomes steady and advances with a nearly constant velocity and height (Gladstone et al., 1998). The slumping phase dominates until the depth ratio of the intruding fluid to

the intruded one is reduced to less than 0.075 (Huppert and Simpson, 1980). Subsequently, the flow enters into a third phase characterised by a balance between the buoyancy and inertial forces of the flow. This phase is termed the inertial phase. This is followed by a viscous phase, wherein the viscous forces balance the buoyancy force.

An example of gravity flow, which is of a significant importance to the oil and gas industry sector is the catastrophic failure of above-ground storage tanks, wherein the whole containment escapes the tank in a sudden manner. The hazard is exacerbated if the escaped material is hazardous and flammable or if it causes other tanks to fail resulting in what is termed a domino effect (Schmidt, 2017). There are many causes that can trigger the failure of storage tanks, including natural disasters. Some countries experience extreme climatic conditions or geological phenomena, such as earthquakes and hurricanes. For example, in the wake of Hurricane Katrina that hit the Gulf Coast in 2005, where many sudden catastrophic failures occurred (Atherton and Ash, 2007). Furthermore, the release of a large quantity of oil occurred due to crack propagation in the wake of an earthquake that hit Shiogama, Japan in 1978 (Chang and Lin, 2006).

---

* Corresponding author.
E-mail addresses: megdich_islem@yahoo.fr (I. Megdiche), C.B.Harris@ljmu.ac.uk (C. Harris).

Additionally, defects such as corrosion, craks, etc., can cause the catastrophic failure of a storage tank. In a study by Chang and Lin (2006) that investigated the causes of 242 failures of storage tanks for a period ranging from 1960 to 2003, cracks and corrosion resulted in the failure of 17 tanks and welding defects were found to be the main cause of 18 failures. The reader is referred to (Chang and Lin, 2006) for more possible causes of catastrophic failures.

The consequences of the sudden failures of storage tanks are very severe. Failures have impacts on the environment, human health, and the economy. Catastrophic failures are usually associated with intense after-effects. In a study conducted by Gyenes and Wood (2014) on the impacts of major accidents involving storage tanks on the environment, it has been shown that 86 out of 687 major accidents occurring between 1986 and 2013 in the EU and the Organisation for Economic Cooperation and Development (OECD) countries had serious effects on the environment. Threats to the environment cover pollution of rivers, sea, soil, air, etc. The impacts on the environment can have implications for the immediate community by contaminating the air, the water, fish, and other food sources. Moreover, the accidents can cause a disruption of the livelihood of the people living in the affected area. In some cases, there were orders of emergency evacuation of people and closure of local infrastructure such as motorways, hospitals, and schools (Atherton, 2008). The losses in some accidents were deemed very high and had major impacts on the economy. For example, after the failure of a storage tank in Buncefiled, UK in 2005, where losses were estimated at £10,000,000 in stored material (Atherton, 2008).

In many storage sites, where potentially polluting materials are handled, the primary containment (storage tank) is surrounded by a secondary containment referred to as a bund wall. This is for the purpose of containing any spillage, should the primary containment fails. A bund wall is a facility that consists of a wall and base, which is structurally independent from the primary containment. Bund walls are commonly constructed from earth, brickwork, reinforced concrete and in some old facilities, they are made from plain concrete. Concerning their capacities, the adopted practice in the UK industries is that a bund wall has to hold 110% of the capacity of the storage tank in case of individual bundling or 25% of the total capacity of the storage tanks if two tanks or more are provided within the same bund wall, whichever is greater (Ash, 2010; Walton, 2014).

The modelling of the catastrophic failure of storage tanks has been a topic of interest for so many years using various approaches. Physical modelling has been widely applied to quantify mainly the overtopping quantities and dynamic pressures (Greenspan and Young, 1978; Greenspan and Johansson, 1981; Thyer et al., 2002; Pettitt and Waite, 2003; Kleefsman et al., 2004; Atherton, 2008; Ash, 2010; Luan et al., 2020). As an example, Atherton (2008) conducted hundreds of tests using a test facility constructed to the scale of 1:30. The research covered a range of bund wall geometries (circular, triangular, square, and rectangular), four bund wall capacities (110%, 120%, 150%, and 200%) and three groups of tanks (tall, middle, and squat) corresponding to ratios of tank radius to fluid height of 0.5, 1.0, and 2.5, respectively. Atherton (2008) demonstrated that for bund walls of 110% capacity, overtopping losses of 70% were obtained and the dynamic pressures were in excess of 16 times the hydrostatic pressure. The effect of mitigation measures was addressed experimentally in Ash (2010) by changing the design of the tank and bund wall. The mitigation measures incorporated were Mitigation of Tank Instantaneous Failure (MOTIF) and Catastrophic Overtopping Alleviation of Storage Tanks (COAST). MOTIF is implemented by adding a baffle inside the tank of a height of one third of the fluid height, while COAST is implemented by fitting a baffle at the top of the bund wall. Using MOTIF allows a reduction in losses between 73% and 80%, 60% and 73%, 34% and 55% for squat, middle, and tall tanks, respectively. The inclusion of COAST allowed a reduction between 15% and 60% in the case where the capacity remains at 110%, while a reduction between 21% and 74% in case where COAST is incorporated as retrofit, thus increasing the bund capacity. Combining COAST and

MOTIF allows a considerable reduction, varying between 70% and 98% for the range of configurations considered.

Beside the physical modelling, CFD is a powerful tool that allows simulation of the complex physics of the catastrophic collapse of storage tanks. It is possible to investigate the effect of various factors without the need of conducting experimental work for each case. Experimental work can be expensive, time consuming or in some cases dangerous to carry out, especially if hazardous materials are involved. However, CFD results are prone to various errors such as modelling and numerical errors. Therefore, a validation of numerical results is needed. CFD modelling of the catastrophic collapse was subject to several studies (Greenspan and Young, 1978; Trbojevic and Slater, 1989; Kleefsman et al., 2004; Ivings and Webber, 2007; Nair, 2008; Ash, 2010; Megdiche et al., 2017; Liu et al., 2017; Ramajo et al., 2018; Huo et al., 2021, 2022).

Some models are based on Shallow Water Equations (SWE) such as SPreading Liquid Over Terrain (SPLOT) developed by Webber and Ivings (2010) and the Liquid Spill Modelling System (LSMS) developed by Cambridge Environmental Research Consultants (Webber et al., 2009). The SWE theory is derived from the 3D fluid dynamics equations and is valid for cases where vertical accelerations are small. Both models exhibit some weaknesses to an extent. The LSMS model considerably overpredicts the overtopping fractions for medium values of kinetic energy and the SPLOT model shows discrepancy as compared to experimental overtopping for situations where the liquid impacts the bund wall with a sufficiently high velocity and turns upwards reaching a height greater than the bund height. Also, the SWE is used for inviscid flows and do not allow for friction modelling. As a result, overtopping fractions are overestimated as shown in Liu et al. (2017). CFD models appear to better predict the flow and yield more accurate estimation of overtopping quantities (Liu et al., 2017; Ramajo et al., 2018). Liu et al. (2017) simulated the catastrophic failure of a storage tank in an oil depot in China using Ansys Fluent to investigate the influence of tank volume, oil property, height of the dike, tank group layout, and rupture form on the overtopping fractions. Unlike in the UK, the capacity of a bund wall in China is equal to 100% plus 0.2 m added to the real height of the bund. It has been shown that overtopping fractions increase with larger tank volumes, lower bund heights, and lighter oils and that the best arrangement allowing minimum quantities of overtopping is the square arrangement with multiple tanks when compared to a cross arrangement which is a square layout with a single tank in the middle. The overtopping fractions are 47.2% for square arrangement while they are 48.4% for a cross arrangement. Megdiche et al. (2017) run extensive simulations to model the catastrophic collapse of a storage tank using the InterFoam solver of OpenFoam software. The numerical model was tested against 13 physical cases covering various separation distances between the tank and the bund wall, bund wall capacities, bund wall heights, shapes of the bund wall, fluid heights, and temperatures of the stored material. This was for the purpose of gaining confidence in the solver. Two quantities were used for the validation, which are overtopping fractions and dynamic pressures at various locations. The dynamic pressures were measured at the centre line, quarter line, and end line of the wall. The end line lies next to the corner of a 90° quadrant. In order to evaluate the performance of the solver, a simulation was considered good for a relative error between 0% and 15%, average for a relative error between 15% and 50%, and weak for a relative error beyond 50%. It has been demonstrated that InterFOAM was able to give good results of dynamic pressures at 38.53%, average results at 43.12% and weak results at 18.34%. For overtopping fractions, InterFoam gave good predictions at 58.53%, average predictions at 21.95%, and weak predictions at 19.51%. The best results obtained correspond to the cases where the bund wall is sitting less than 0.7 m from the tank. Huo et al. (2021) addressed the overtopping of circular bunds using Ansys Fluent. The turbulence was modelled using RNG $k - \varepsilon$ and LES models and the modelling space was limited to 2D. It has been shown that the LES model outperforms the RNG $k - \varepsilon$ model in predicting the overtopping quantities, the flow behaviour, and the physical interaction between the flow

and the bund. However, the use of a 2D model is ineffective for other shapes of the bund wall, such as rectangular and square walls. Therefore, Huo et al. (2022) extended their CFD model to the 3D space and square bund walls using the same turbulence models for the purpose of estimating the dynamic pressures in addition to the overtopping fractions and the flow behaviour. Contrary to the case of a 2D model, $k - \varepsilon$ performs better than LES model. The advantages of a 3D model versus a 2D model consists in capturing the secondary overtopping process, while only one overtopping process was possible to see with a 2D model. Additionally, it shows the dynamic interaction between the flow and the bund wall. The research of Huo et al. (2022) shows that pressures are larger at the bottom than at the top, greatest in the corners for a square bund wall, and higher for a square bund wall as compared to a circular bund wall for the same filling ratio.

Research investigating the effect of mitigation measures on the catastrophic failure of storage tanks is very rare. One pioneer work is of Ash (2010) in which the effect of including mitigation measures was addressed via the use of STAR-CCM^{+}. The mitigation measures incorporated are COAST and MOTIF. The error in numerical results is very significant reaching up to 378% for overtopping fractions and 3571% for dynamic pressures. Ramajo et al. (2018) investigated the effect of adding top wall deflectors under various modes of failure using OpenFOAM, where the liquid depth is 0.6 m, the bund height is 0.12 m, the bund capacity is 110%, and the breakwater width is 20% of the bund height. Five breakwaters were implemented to the square wall which are: Horizontal breakwater (H - BW), inclined breakwater (I - BW), a combination of horizontal and one vertical breakwaters where the vertical one lies in the middle of the bund (H + V - BW), a horizontal and two vertical breakwaters (H+2 V - BW), and a combination of a small roof on the corner, a horizontal and a vertical breakwater (H'+V - BW). For the circular wall, only a horizontal breakwater is added. The overtopping fractions Q for the circular wall is 6.56% with a breakwater incorporated as compared to 47.66% for a standard configuration. For the square wall, the highest reduction is for the case of a (H'+V - BW) with Q = 8.79%, followed by (H + V - BW) with Q = 9.79%, and (H+2 V - BW) with Q = 10.42% against Q = 48.55% for the unmitigated bund wall. On the contrary, inclined and horizontal breakwaters do not contribute significantly in reducing the losses with Q = 12.39% for (H - BW) and Q = 19.61% for (I - BW). Breakwaters investigated in Ramajo et al. (2018) reduced the losses to some extent, but important quantities of fluid still escape the bund wall. Another main concern is the additional weight that these breakwaters will induce on the wall which makes it susceptible to failure. By comparing the works of Ramajo et al. (2018) and Liu et al. (2017), there is a discrepancy in the obtained results. Ramajo et al. (2018) found that overtopping fractions are larger in case of vertical bottom hole compared to the case of cross rectangular hole, while Liu et al. (2017) reached the opposite conclusion. This questions the validity of the results of Ramajo et al. (2018) in the case of incorporating breakwaters. Also, according to Huo et al. (2022), the model of Ramajo et al. (2018) lacks validation, as it was only validated against two cases (the circular and rectangular walls with a fluid height of 0.6 m).

In Liu et al. (2017); Ramajo et al. (2018); Huo et al. (2021, 2022), only the overtopping fractions and the flow behaviour were used for the validation of numerical results against experimental results, while clearly ignoring the dynamic pressures, which are very important to consider if the structural integrity of the wall is to be addressed. In Liu et al. (2017), it was clearly mentioned that the calculation of the impact values compare poorly to the experimental results and this was attributed to the fact that the algorithm is not mature for these kinds of problems. In Ramajo et al. (2018), ignoring the dynamic pressures was attributed to the fact that the geometry and the location of probes were ambiguously reported. However, in Megdiche et al. (2017), both of overtopping fractions and dynamic pressures were used for validation.

Therefore, it is imperative to use a well validated model and design appropriate mitigation measures that significantly reduce the overtopping fractions and dynamic pressures, hence mitigating the

Table 1
Errors in CFD results from Ash (2010).

Test type	Errors from initial methodology	Errors from revised methodology
Standard	$20.3\% \leq Q_{diff} \leq 78.6\%$	$-11.92\% \leq Q_{diff} \leq -3.44\%$ $327\% \leq P_{diff} \leq 1089\%$
MOTIF	$-0.08\% \leq Q_{diff} \leq 34.14$	$11.55\% \leq Q_{diff} \leq 89.33\%$ $353\% \leq P_{diff} \leq 2842\%$
COAST	$50\% \leq Q_{diff} \leq 378\%$	$-79.52\% \leq Q_{diff} \leq -49.52\%$ $528\% \leq P_{diff} \leq 3571\%$
MOTIF and COAST	$Q_{diff} = 41\%$	$49.4\% \leq Q_{diff} \leq 64.9\%$ $80\% \leq P_{diff} \leq 96\%$

consequences of the sudden failure of a storage tank. This work uses the CFD model developed in Megdiche et al. (2017) as it gave good results for many of the standard configurations. The mitigation measures (MOTIF and COAST) are incorporated. The mitigation measures are optimised to reduce the overtopping fractions and dynamic pressures. The effect of mitigation measures for different capacities, shapes of bund walls, and heights of fluid is addressed by comparing the dynamic pressures and overtopping quantities against those corresponding to standard cases. This work will serve as a guidance for stakeholders in the process industry on the bund design as part of risk assessment.

This paper is organised as follows: Section 2 presents the theoretical background of this research. Section 3 presents the experiment that served to validate the numerical results of the standard configurations (Megdiche et al., 2017). The numerical results of dynamic pressures and overtopping fractions of the mitigated configurations are compared with the experimental results. Section 3 also presents the investigated configurations. Section 4 provides the numerical method utilised in detail. Section 5 firstly presents the results of the optimisation study that permits the selection of the appropriate mitigation measure, along with the discussion the effect of incorporating the optimised mitigation measure on the overtopping quantities and dynamic pressures using different capacities, shapes of bund walls, and heights of stored fluid. Section 6 provides the major conclusions of this work.

2. Theoretical background

Ash (2010) and Atherton (2008) are considered benchmark studies for the current research, as they used the same test rig and similar test configurations. For running CFD simulations, Ash (2010) used STAR-CCM^{+} version 3.02.003 installed on a computer with an Intel Core 2 Duo T7500 processor, and considered an angular slice of the computational domain instead of the full 90° quadrant. The range of angular slices tested covered 6, 9, 12, 15, 18, 45 and 90°. The 15° model was retained for further numerical analysis, as smaller slices influenced the mesh density, while 45 and 90° slices took considerable time to run. Ash (2010) employed two different methodologies: in the initial one, built in functions were used to determine the volume of fluid surpassing the bund, this methodology allowed only the calculation of the overtopping fractions. In the revised methodology, a wave averaging technique was employed along with virtual instruments such as depth gauges and dynamic pressure probes, this methodology allowed both of overtopping fractions and dynamic pressures to be determined. Regarding the turbulence modelling, the realizable $k - \varepsilon$ model was adopted. CFD simulations were run for standard configurations, configurations incorporating MOTIF, configurations incorporating COAST, and configurations incorporating MOTIF and COAST, using circular middle tanks. Errors (Q_{diff} and P_{diff}) in overtopping fractions and dynamic pressures between experimental and numerical results are presented in Table 1. Positive and negative errors mean the quantities are overestimated and underestimated, respectively. It appears that the revised methodology worked better than the initial methodology only in the case of standard configurations to predict the overtopping fractions, however it failed to provide exact values of dynamic pressures. The
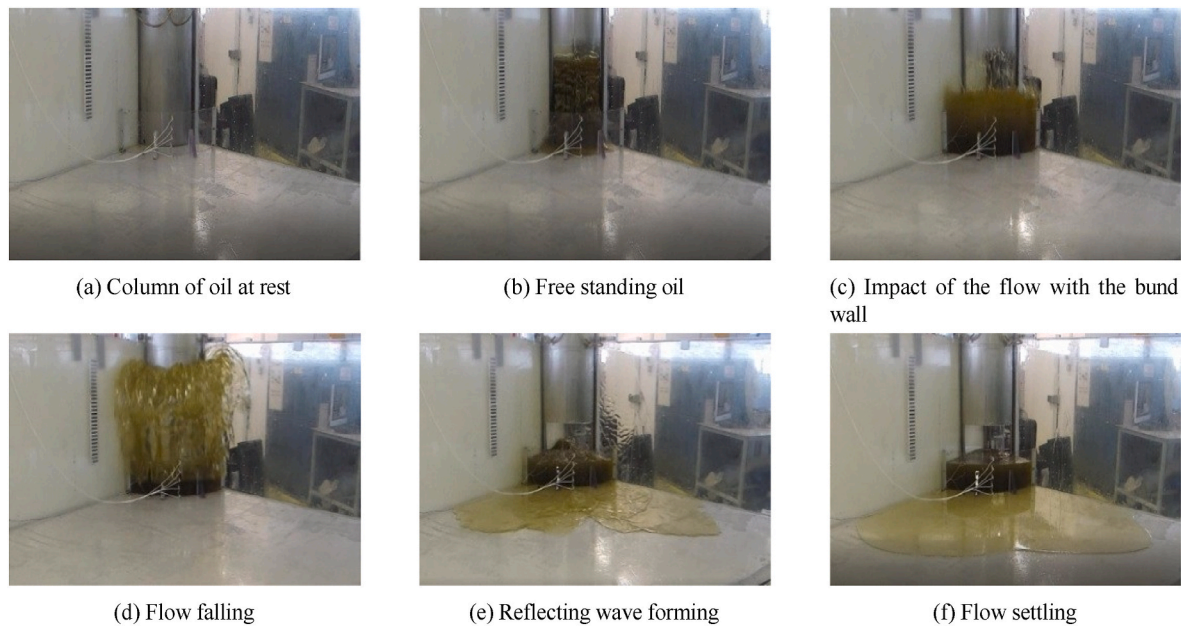
(a) Column of oil at rest

(b) Free standing oil

(c) Impact of the flow with the bund wall

(d) Flow falling

(e) Reflecting wave forming

(f) Flow settling

Fig. 1. Experiment of the collapse of an above-ground storage tank.

initial methodology worked better than the revised methodology for cases incorporating MOTIF to predict overtopping fractions. Overall, it can be noticed that both methods are not reliable, especially to predict the dynamic pressures as an error of 3571% was attained. According to Ash (2010), the discrepancy in the results is attributed to anomalies in the software, limitations in computing power, and the license period of the software that was only valid for one year, which limited the mesh resolution used. To overcome these issues, OpenFoam was favoured to run the simulations, since it gave good results in Megdiche et al. (2017), in addition to the fact that it is an open source software. Furthermore, to decrease the computing time, the supercomputer "STOKES" at LJMU was used which consists of 8 nodes with each node being composed of 28 cores. A total of 196 cores were used allowing to decrease the simulation of each case to 2 h. Problems quoted in Ash (2010) related to turbulence modelling and mesh resolution were treated with care as explained in 4.1 and 4.3. The computational domain consists of the full 90° quadrant, as opposed to Ash (2010), to allow more realistic simulation, as the interaction of the escaping fluid with the bounding walls could influence the results. Also, simulating only a fractional slice is possible only in the case of cylindrical bund walls, however, in this paper various shapes were simulated apart from other parameters, namely different capacities and heights of the fluid. The estimation of the overtopping fractions was performed using filters in the post-processing software ParaView that isolates the region outside the bund wall and computes the volume of fluid occupied by the cells, a methodology similar to the first methodology used by Ash (2010). Dynamic pressures were computed using the probe filter in Paraview. Dynamic pressures are of great importance, unlike in Ash (2010), where the primary focus was on determining the overtopping fractions, as the structural integrity was to be studied in a subsequent research.

3. Definition of the reference test case

Extensive experimental work on the catastrophic failure of storage tanks was carried out within a previous research project that took place at Liverpool John Moores University. The testing was carried out to investigate the behaviour of the collapse with different capacities of bund wall, using multiple heights of fluid, and various shapes of wall. The experiments were carried out at a scale of 1:30 (Atherton, 2008). The experiment as depicted in Fig. 1 consisted of the removal of a tank quadrant. This is fulfilled by accelerating it upwards using a power/spring cord at an initial rate of 250 ms^{-2} (Atherton, 2008). This allows the flow to rapidly escape under the effect of gravity. The flow moves forward until it impacts the bund wall. Subsequently, the flow moves
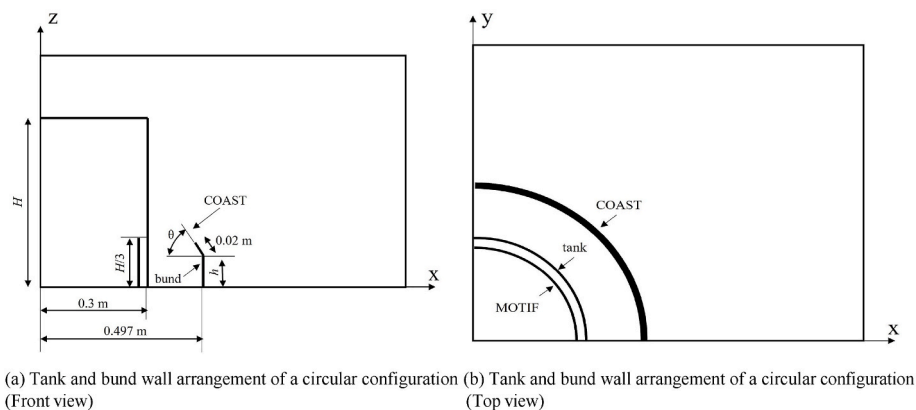

(a) Tank and bund wall arrangement of a circular configuration (Front view)

(b) Tank and bund wall arrangement of a circular configuration (Top view)

Fig. 2. Schematic of the tank, bund wall and mitigation measures with the dimensions (not true to scale), MOTIF is located at 0.03 m from the internal face of the tank.

Table 2

Test matrix for circular bund walls incorporating mitigation measures ($H = 0.6$ m).

	Test name	Angle (degrees)	Capacity %	r (m)	h (m)
Optimisation of the angle of the baffle	$M\&C_{10}$	10	110	0.497	0.24
	$M\&C_{20}$	20	110	0.497	0.24
	$M\&C_{30}$	30	110	0.497	0.24
	$M\&C_{40}$	40	110	0.497	0.24
	$M\&C_{50}$	50	110	0.497	0.24
	$M\&C_{60}$	60	110	0.497	0.24
	$M\&C_{70}$	70	110	0.497	0.24
	$M\&C_{80}$	80	110	0.497	0.24
Selection of the mitigation technique	M	–	110	0.497	0.24
	C_{45}	45	110	0.497	0.24
	$M\&C_{45}$	45	110	0.497	0.24
Effect of capacity	$C_{80} - 110\%$	80	110	0.497	0.24
	$C_{80} - 120\%$	80	120	0.52	0.24
	$C_{80} - 150\%$	80	150	0.581	0.24
	$C_{80} - 200\%$	80	200	0.671	0.24

Table 3

Effect of COAST using non-circular bund walls ($H = 0.6$ m).

Test name	Shape	d_x (m)	d_d (m)	h (m)
$C_{80} - triangular$	triangular	0.582	0.324	0.12
$C_{80} - square$	square	0.324	0.582	0.12
$C_{80} - rectangular$	rectangular	0.141	0.686	0.12

Table 4

Effect of COAST using different heights of stored material (Capacity = 110%, r = 0.497 m).

Test name	H (m)	h (m)
$C_{80} - tall$	0.6	0.24
$C_{80} - middle$	0.3	0.12
$C_{80} - squat$	0.12	0.047

upward and droplets are formed. When a certain height is attained corresponding to a maximum potential energy, the flow starts falling back and reflective waves are formed. Part of the flow stays in the bundled area and the rest moves forward outside the bund wall until it comes to rest.

In this work, a configuration that gave good results for overtopping fraction and dynamic pressures in Megdiche et al. (2017) is selected for the optimisation of mitigation techniques. The selected test uses a tall tank, a circular bund wall located at 0.497 m from the centre of the tank, and a capacity of 110%. The relative error obtained from this test is below 5% for both dynamic pressures and overtopping fraction. The height of MOTIF is chosen to be the same as in Ash (2010), which has a height of $H/3$, where H is the height of the fluid. COAST is incorporated as a retrofit to the wall by fitting a 20 mm straight inwardly facing baffle. Ash (2010) used baffles inclined at 45°, while in this study the angle of inclination Θ is optimised. Θ covers angles ranging from 10 to 80° with an increment of 10° being performed on configurations incorporating MOTIF and COAST together. The mitigation techniques and bund wall arrangement along with dimensions are given in Fig. 2.

Furthermore, the performance of each mitigation measure is investigated separately and compared to the case when both MOTIF and COAST were incorporated at an angle of 45°. This is for the purpose of selecting the appropriate mitigation technique which allows a reduction in the dynamic pressures and overtopping quantities at a reduced cost. Subsequently, the effect of using the optimised mitigation measure on bund walls with different capacities, shapes, and heights of the stored

material is considered. This is to allow comparison against standard configurations, where the experimental data sets are available. The dimensions and the specifications of the different tests are illustrated in Tables 2–4. H is fluid height, r is the radius of the bund, h is the bund wall height, d_x is the separation distance along the x axis and, d_d is the separation distance in the diagonal direction. $M\&C$ is a test incorporating MOTIF and COAST, M is a test incorporating MOTIF only, and C is a test incorporating COAST only (Megdiche, 2019).

4. Numerical method and setup

4.1. Mathematical models

The Volume of Fluid (VOF) approach falls under the volume tracking method and is extensively used to model a multiphase flow problem (Heyns and Oxtoby, 2014). It is based on considering an indicator function (α) which represents the volume fraction of the fluids in the cell grid. If α is the volume fraction of the liquid, then $\alpha = 1$ for a cell occupied by the liquid, $\alpha = 0$ for a cell occupied by the gas and $0 < \alpha < 1$ if the cell is occupied by the liquid and the gas. The VOF is based on constructing an advection equation for the volume fraction that describes the evolution of the free surface, it reads:

$$\frac{\partial \alpha}{\partial t} + \nabla.(\alpha U) = 0 \tag{1}$$

For a multiphase flow, it is necessary to include the surface tension forces in the conservation of momentum equation. These forces act at the interface of the different phases of the flow. By accounting for the surface tension, the Navier-Stokes equation becomes:

$$\frac{\partial \rho_m U}{\partial t} + \nabla.(\rho_m UU) = \rho_m g - \nabla p + \mu_m \nabla^2 U + \int_{\Gamma_{lg}} \sigma_s k\delta(x - x_s)n \, d\Gamma_{lg}(x_s) \tag{2}$$

where σ_s is the surface tension, z is the interfacial curvature, $\delta(x - x_s)$ is the 3D Dirac delta function, n is the normal vector to the surface, and Γ_{lg} is the liquid-gas interface. The viscosity μ_m and the density ρ_m are those corresponding to the mixture of the two phases, they are given by

$$\rho_m = \alpha\rho_1 + (1 - \alpha)\rho_2 \tag{3}$$

and

$$\mu_m = a\mu_1 + (1 - \alpha)\mu_2, \tag{4}$$

where ρ_1, ρ_2, μ_1, and μ_2 are the densities and the dynamic viscosities of the liquid and the gas, respectively (Deshpande et al., 2012).

In order to predict the wall behaviour, the flow must be resolved up to the wall by using a very fine mesh in such a way the first node is located inside the viscous sublayer, this approach necessitates the use of Low Reynolds Number (LRN) models (Bredberg, 2000). Therefore, the Shear-Stress Transport ($k - \omega-$ SST) model (Menter et al., 2003) in its low Reynolds version is chosen for turbulence modelling due to its ability to predict flows with adverse pressure near the wall and avoid the sensitivity to the values of ω outside the boundary layer. Reynolds number (Re) is equal to $L.U/v$, where L, U, and v are a characteristic length, a characteristic velocity, and the kinematic viscosity, respectively. In this case, L is taken as the separation distance between the tank and the bund wall ($L = 0.197$ m), $U = 4.53$ m/s from Atherton (2008), and $v = 67.4 \ 10^{-6} \ \text{m}^2/\text{s}$. This gives $Re = 13,240$ which is considered a low value. Problems in this range of Re numbers were simulated using low Reynolds number turbulence models (Menni et al., 2016; Aftab et al., 2016).

4.2. Physical properties of the fluids

The physical properties needed to calibrate the material models in

Table 5

Physical properties of the fluids (Sahasrabudhe et al., 2017).

Fluid	Density ρ_f (kg/m^3)	Kinematic viscosity v (m^2/s)
air	1.1839	15.57 10^{-6}
olive oil	910.9	67.4 10^{-6}

InterFoam are the density and the kinematic viscosity of olive oil and air, which are considered as Newtonian fluids. Additionally, the surface tension between olive oil and air is also required. At 25 °C, the value of the surface tension between the fluids is 0.025 (Sahasrabudhe et al., 2017). The values of density and kinematic viscosity for olive oil and air at 25 °C are given in Table 5.

4.3. Mesh

The computational domain is created in Salome 7.8.0 with the same dimensions as the experimental set-up, and is depicted in Fig. 3a, b, and c. The mesh is built ensuring certain rules of quality such as smoothness and aspect ratio. The mesh created is structured with hexahedral cells and a few prisms in the corner and the grid lines are aligned with the flow as much as possible. The reason behind this is that hexahedral mesh yields a more accurate solution in the case of alignment of the grid lines with the flow direction. A transition ratio of 1.2 is not exceeded to ensure a reasonable level of smoothness. Additionally, the aspect ratio is reduced as much as possible, except in near wall regions, where a high aspect ratio of 800 is used to reduce the cell count, while satisfying the y^+ condition. The height of cells near the wall were of the order of 10^{-4} m. OpenFOAM allows an aspect ratio up to 1000 and cells with high aspect ratio near the wall are commonly used to reduce the cell count and is acceptable as long as the flow is aligned with the longest side of the cell. There are other mesh quality rules such as skewness and orthogonality, etc. OpenFOAM has a utility called CheckMesh to ensure that a mesh meets the requirements before starting a simulation. All meshes are checked before running any case. The $y^+ = 1$ criterion was satisfied on the base and the bund wall, which resulted in a dense mesh next to these regions. Ultimately, the cell count reaches up to 4.9 million cells.

4.4. Discretisation schemes

The discretisation schemes of the different terms of the transport equation of the multiphase flow are summarised in Table 6. The default schemes proposed in OpenFOAM are adopted due to their suitability to simulate the physics, i.e. the diffusion is an isotropic phenomenon, therefore a central (linear) scheme is used for the discretisation of the diffusion term. The convection term in the N-S equation is discretised using a LinearUpwind scheme, which allows the determination of the

flux from the direction of the flow (Megdiche, 2019).

4.5. Boundary conditions

The boundary conditions used in this problem consist of wall and atmosphere types. The wall type is adopted for the surrounding walls and the base of the computational domain, while the atmosphere type is applied to the top boundary of the domain, which is free to the atmosphere. The types of numerical boundary conditions of each computed
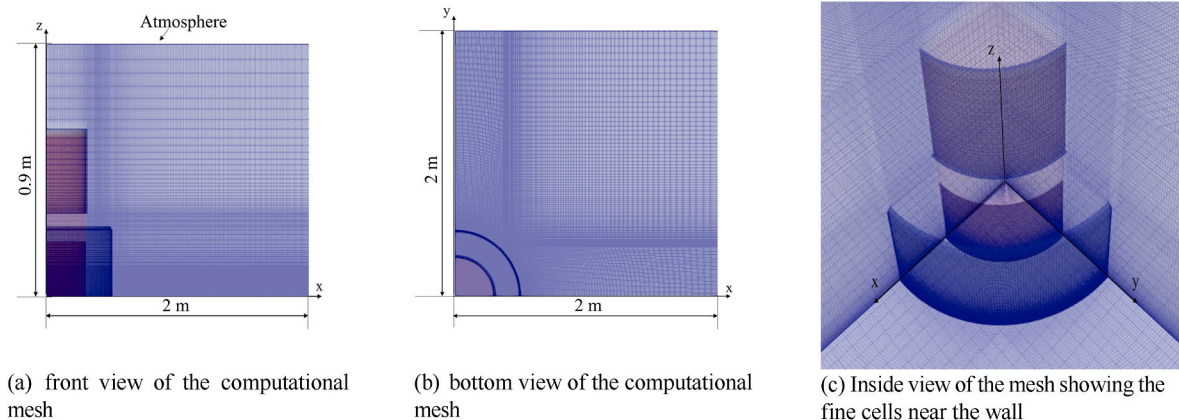
Table 6

Discretisation schemes.

Term		Family of discretisation scheme	Discretisation scheme	
			Discretisation scheme of volume integrals	Interpolation scheme
Temporal term		ddt schemes	–	Euler
Pressure term		grad schemes	Gauss	linear
Diffusion term		laplacian schemes	Gauss	linear corrected
Convection terms	N-S equation phase fraction equation			linearUpwind vanLeer
	Interfacial compression flux	div schemes	Gauss	linear
	k transport equation			upwind
	ω transport equation			upwind
	Reynolds stress term			linear

Table 7

Types of boundary conditions for the different variables.

Variables	Wall	Atmosphere
Pressure	"fixedFluxPressure"	"totalPressure"
Velocity	"fixedValue"	"pressureInletOUtletVelocity"
Volume fraction α	"zeroGradient"	"inletOutlet"
Turbulent kinetic energy k	"KLowReWallFunction"	"inletOutlet"
Specific dissipation rate ω	"omegaWallFunction"	"inletOutlet"
Kinematic turbulent viscosity v_t	"nutLowReWallFunction"	"calculated"

(a) front view of the computational mesh

(b) bottom view of the computational mesh

(c) Inside view of the mesh showing the fine cells near the wall

Fig. 3. Computational mesh of a circular bund wall configuration with the dimensions.

(a) Dynamic pressure

(b) Overtopping fraction
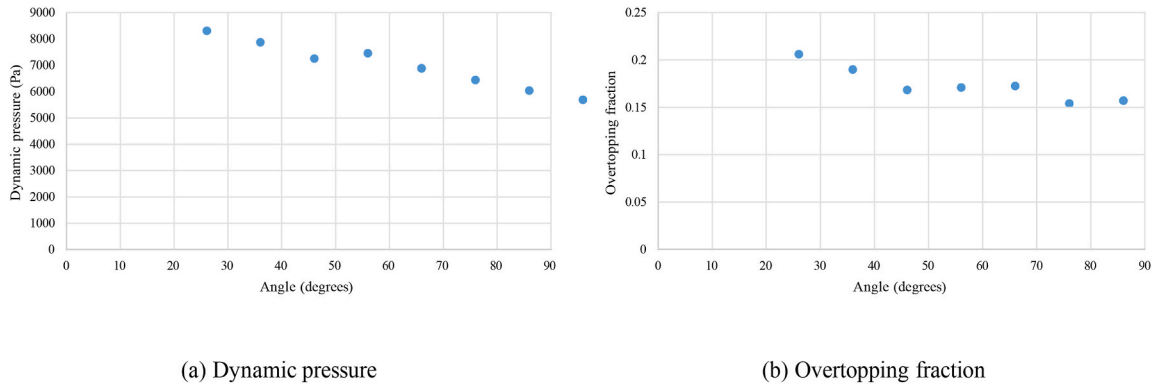
Fig. 4. Dynamic pressure and Overtopping fraction of various inclination angles of COAST.

(a) Front view of the sensor location
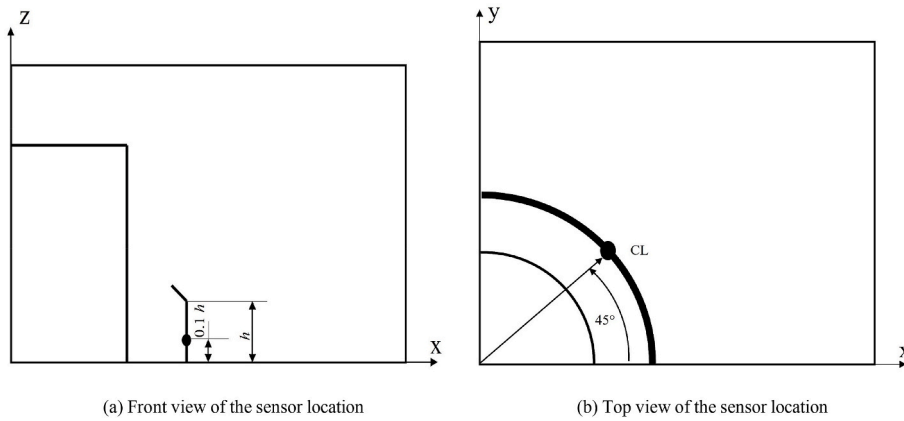
(b) Top view of the sensor location

Fig. 5. Schematic of the transducers location along the bund wall (not true to scale), (a) Front view showing that the transducers are located at 10% from the base (b) Top view showing that the transducer is located at the centre line of the quarter of the tank.

term are given in Table 7. It is assumed that the walls are impermeable, hence the use of the zero gradient boundary condition for the volume fraction and a fixed flux pressure set to zero for the pressure term. The velocity is considered to adhere to the walls due to viscous effects, therefore a fixed value set to zero is chosen for the velocity. For the atmosphere boundary, a combination of boundary conditions for the different terms allows the inflow and outflow according to the internal flow (Greenshields, 2018).

4.6. Numerical model and solution procedure

InterFoam uses the semi-implicit Multidimensional Universal Limiter for Explicit Solution (MULES) for the discretisation of the phase fraction equation. In order to solve for a transient two-phase flow in OpenFOAM, the advection equation of the phase fraction needs to be solved first and then the momentum equation is solved through the PISO algorithm. A two-phase flow problem is solved in OpenFOAM as follows (Lopes, 2013):

1. Set all variables to their initial values.
2. Compute the Courant number Co and adjust the time step.
3. Solve the phase fraction equation using the fluxes from the previous time step and calculate the density and viscosity using the new α values.
4. Compute the normal vector n and the local interfacial curvature k.
5. Go through the PISO algorithm until convergence is reached.

The simulations are run for 2s, which is a sufficient time for the fluid flow to settle. An adjustable time step is used with an upper limit on Co equal to 1. The tolerances used for the different terms are 10^{-6} for the

velocity, the turbulence kinetic energy k, and the specific dissipation rate ω, 10^{-7} for the pressure, and 10^{-8} for the phase fraction (Megdiche, 2019).

5. Results and discussions

5.1. Optimisation of the mitigation measure

Fig. 4a and b depict the results of dynamic pressures and overtopping fractions corresponding to different inclination angles of COAST. For the optimisation process, the dynamic pressures are given in terms of the highest values recorded at the wall during the impact. Whereas, for studying the effect of the mitigation measure depending on the capacity, the shape of the wall, and the height of the fluid, the dynamic pressures are measured at a height of 10% from the base and along the centre line (CL), as shown in Fig. 5, as this is where the experimental data sets are available. According to Fig. 4a, the dynamic pressures tend to decrease with increasing angles. Similarly, the overtopping fractions decrease with an increasing angle as depicted in Fig. 4b. However, at an angle 60° and beyond, they become nearly constant. The angle 80° was selected for subsequent simulations because it gave the lowest overtopping fraction and dynamic pressure. The reduction in overtopping fraction compared to the experimental fraction of standard configuration is equal to 18.5%, where the experimental fraction is 0.1837 (Megdiche et al., 2017). However, the dynamic pressure indicates an increase of 15% compared to the experimental dynamic pressure obtained from the standard configuration which is 5,044Pa (Megdiche et al., 2017). This can be attributed to the level of turbulence that increases when the fluid flow hits MOTIF. Furthermore, the dynamic pressure is at its maximum in the vicinity of the deflector as shown in Fig. 6. This is opposed to the
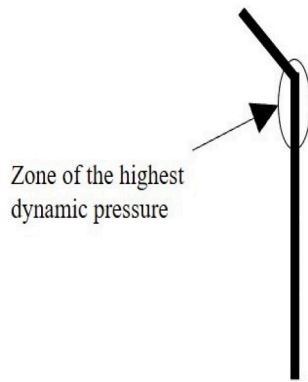
Fig. 6. Zone of the highest dynamic pressure.

case of standard configurations, where the maximum pressure is at the base of the wall. This can affect the structural integrity of the wall as the overturning moment increases.

Therefore, the combination of MOTIF and COAST was questioned on whether MOTIF is really beneficial, especially that it adds to the cost of construction. For this, three simulations were conducted on a circular wall, where the inclination angle is 45°. The three simulations correspond to the use of MOTIF only, COAST only, and MOTIF and COAST combined together. The effect of these various mitigation measures is studied in terms of the flow structure. To better understand this, for each case, an isosurface corresponding to $\alpha = 0.5$ is presented along with a slice of the flow with a normal vector $(-1, 1, 0)$, and a bottom view of the flow. Figs. 7–9 represent the isosurfaces in the case of incorporating MOTIF, the combination of COAST and MOTIF, and COAST, respectively. Figs. 10–12 depict the slices crossing the computational domain diagonally in the case of incorporating MOTIF, the combination of COAST and MOTIF, and COAST, respectively. Figs. 13–15 show a bottom view of the computational domain, for MOTIF, the combination of COAST and MOTIF, and COAST, respectively.

By comparing the isosurfaces and the slices of the configurations incorporating MOTIF and the combination of COAST and MOTIF, it can be seen that up to t = 0.25s the flow structures of both cases are identical

in which the isosurface is convex implying that more fluid is driven outward. At t = 0.35s, COAST serves to revert the flow inward and upward. For the configuration incorporating MOTIF only, the flow slides with respect to the wall until a certain height is attained before it falls downward. At t = 0.75s and beyond, it is visible that the flow is collapsing and a significant fraction of the fluid escapes the bund wall for both configurations. This is opposite to the configuration incorporating COAST only. It can be noticed that for the duration between the collapse and the impact with the wall, the isosurface is concave implying that the flow takes longer to move forward compared to the two previous cases. At t = 0.35s, COAST reverts the flow inward and upward. A comparison between the configurations incorporating COAST and the combination of COAST and MOTIF reveals that at t = 0.75s the flow is still being deflected when using COAST only, but it already starts escaping the bund wall in the case of using MOTIF and COAST. Furthermore, a flow being deflected by COAST can reach higher levels than in the case of using MOTIF and COAST together. COAST also performs to significantly reduce the overtopping fractions as can be seen at t = 2s. This is confirmed by Figs. 13–15, where only minor fractions of overtopping are outside the bund wall, whereas significant overtopping fractions escape the bund wall for a configuration incorporating MOTIF, and to a less extent with a configuration incorporating MOTIF and COAST. Additionally, it can be seen from Figs. 10 and 11, that the flow impacts the top of the wall at a first instance as opposed to the configuration incorporating COAST only, where the flow impacts the base of the bund wall.

Table 8 shows a comparison between the different mitigation techniques in terms of dynamic pressures measured at the bund wall along with overtopping fractions. The dynamic pressure is the lowest in the case of using COAST only and the overtopping fraction is significantly reduced. Incorporating COAST produces an overtopping fraction of 1% compared to 21% for MOTIF only and 17% for COAST and MOTIF combined together. The reduction in overtopping fraction compared to the standard case with the use of COAST only is 94.55%, where the experimental overtopping fraction is 18.37%. Additionally, the overtopping fractions are far below those obtained in Ramajo et al. (2018), where the best value obtained is 6.56%. However, Ash (2010) showed through physical modelling that the combination of MOTIF and COAST is the best option to reduce the overtopping fractions where a reduction

Fig. 7. An isosurface of the flow corresponding to a configuration incorporating MOTIF.

(a) t = 0s   (b) t = 0.2s   (c) t = 0.25s

(d) t = 0.35s   (e) t = 0.75s   (f) t = 2s

Fig. 8. An isosurface of the flow corresponding to a configuration incorporating COAST and MOTIF.

(a) t = 0s   (b) t = 0.2s   (c) t = 0.25s
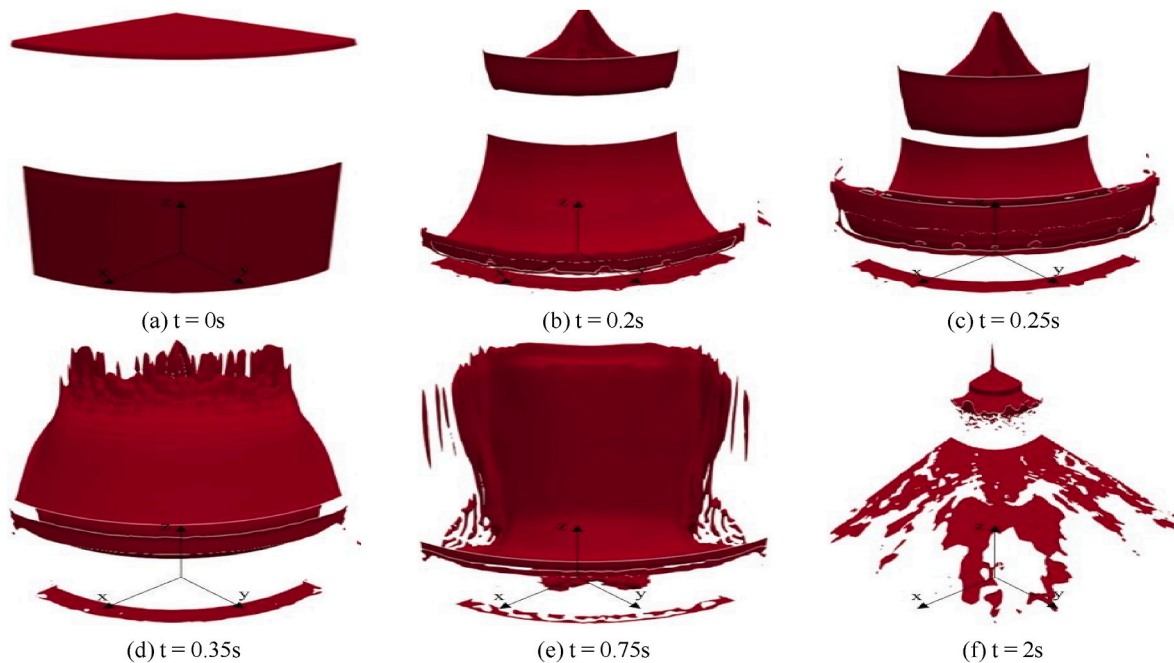
(d) t = 0.35s   (e) t = 0.75s   (f) t = 2s

Fig. 9. An isosurface of the flow corresponding to a configuration incorporating COAST.

between 88% and 98% was achieved using a square bund wall and middle tank arrangements. It is impossible to directly compare the results of this research against Ash (2010) results due to the different bund/tank arrangement. Ash (2010) focused on alleviating the problem of overtopping, while in this research the dynamic pressure is of great importance as the structural integrity of the bund wall was addressed by proposing a design of the bund wall that can withstand the dynamic pressures. As it appears from studying the flow behaviour of the examined configurations, that whenever MOTIF is included the impact of the fluid occurs at the wall in a position that increases the overturning moment. This might not be the case for instances where the bund wall sits at a significant distance from the tank, as the impact might occur

close to the ground. The solution of incorporating MOTIF is impractical in terms of installation and maintenance for exiting tanks, which will require emptying, venting and cleaning at great time and expense. Even in the case of a new tank construction, MOTIF will cause maintenance issues, particularly for inspection and repair of tank walls. Furthermore, the cost of MOTIF is more significant than that of COAST. For all these reasons, COAST only is adopted for subsequent simulations.

5.2. Effect of the incorporation of COAST using different capacities

Fig. 16 presents the effect of incorporating COAST on the dynamic pressures and overtopping fractions using different capacities by
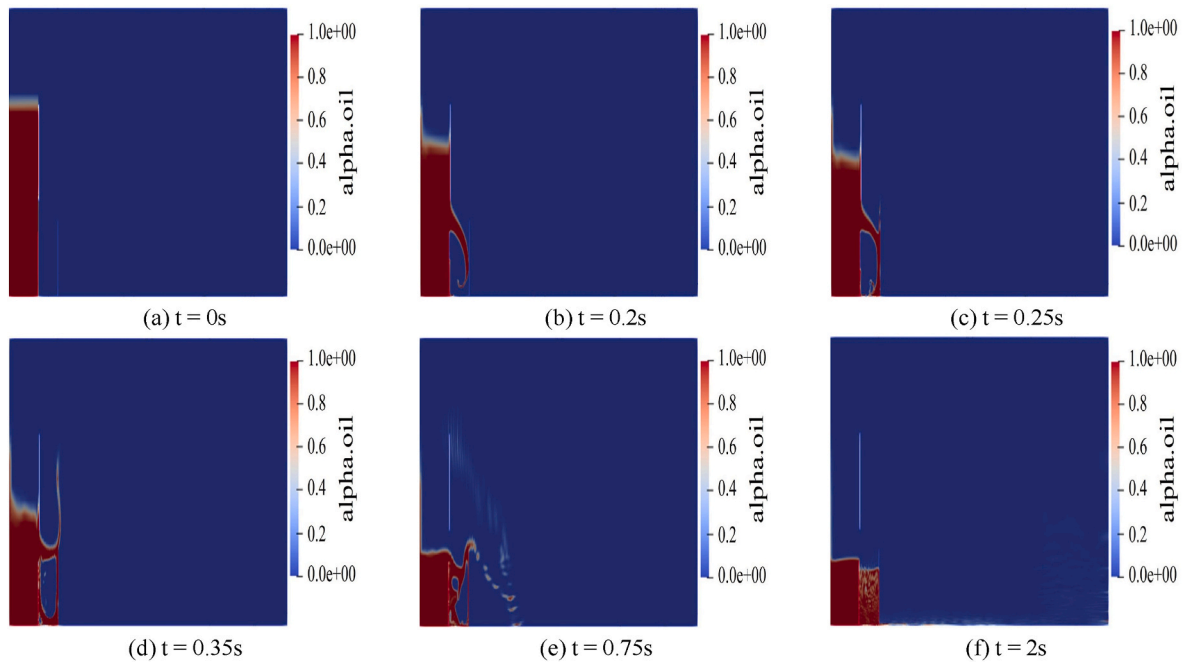
Fig. 10. A slice of the flow corresponding to a configuration incorporating MOTIF.
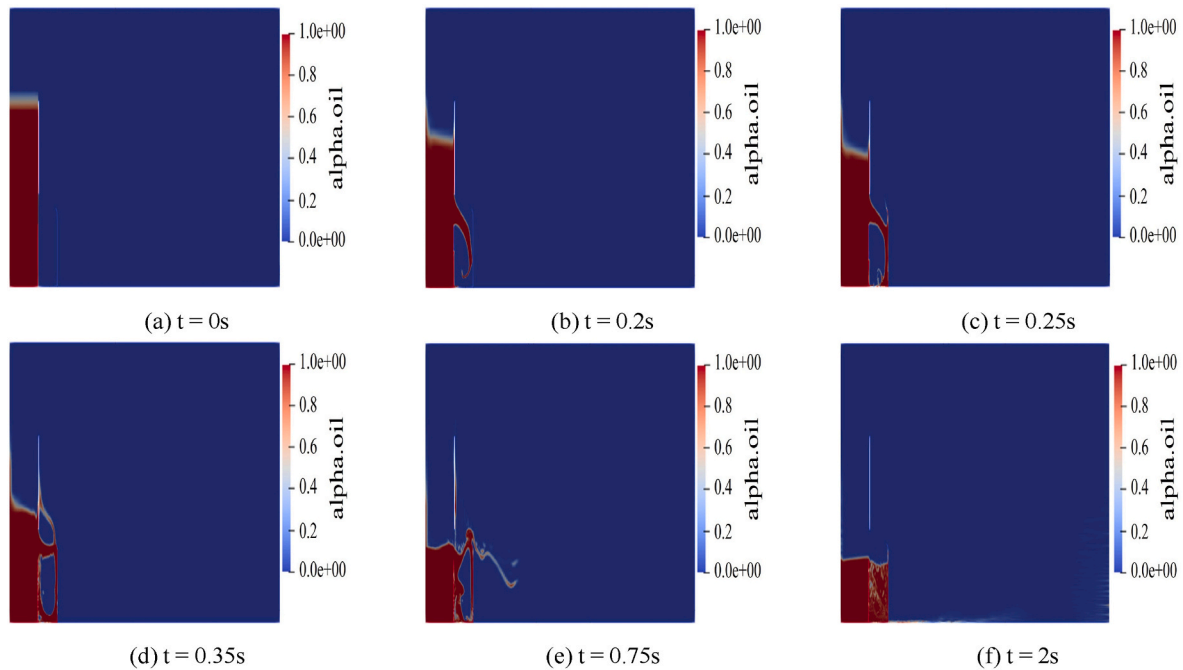

Fig. 11. A slice of the flow corresponding to a configuration incorporating COAST and MOTIF.

comparing them to the experimental results of the standard configurations. The bund capacities are 110%, 120%, 150%, and 200%. The numerical dynamic pressures of mitigated cases employing COAST appear to be greater than the experimental pressures of standard cases. Theoretically, COAST does not change the dynamic pressures, as the flow structures of a standard configuration and a mitigated configuration are similar at the first instant of impact with the wall. The dissimilarity in the pressures is merely related to numerical error. However, the overtopping fractions are significantly reduced. Generally, COAST conserves the same trend of the variation of overtopping fractions with the capacity. The reduction in overtopping fraction is 93%, 94%, 97%, and

98% for capacities of 110%, 120%, 150%, and 200%, respectively.

5.3. Effect of the incorporation of COAST using different shapes of bund wall

Fig. 17 presents the effect of incorporating COAST on the dynamic pressures and overtopping fractions using different shapes. The simulations cover circular, square, rectangular, and triangular bund walls of capacity 110%. Similarly to the previous case, the numerical values are compared against the experimental results of standard configurations, the dynamic pressures should not deviate much from the experimental
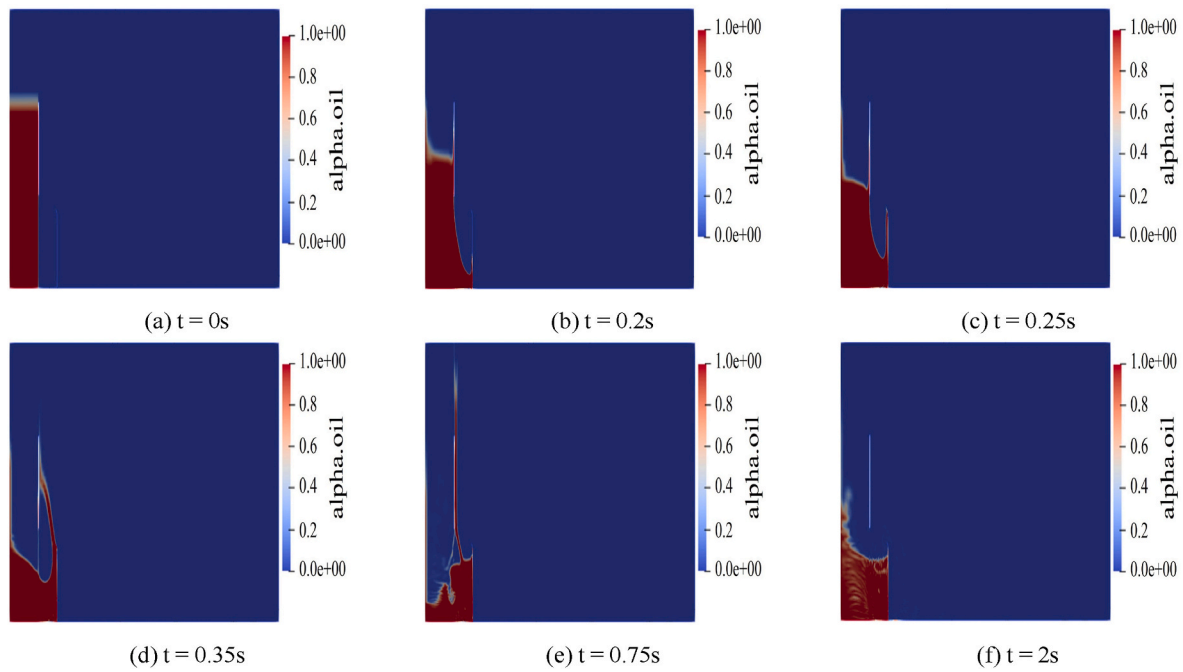
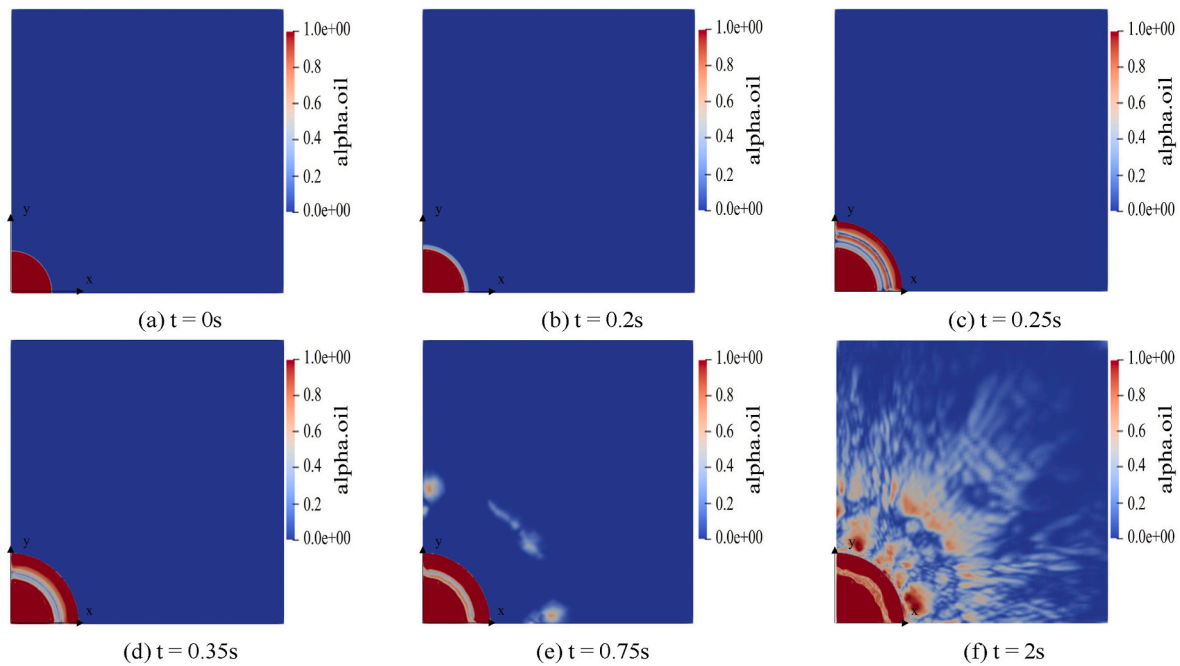Fig. 12. A slice of the flow corresponding to a configuration incorporating COAST.

Fig. 13. A bottom view of the flow corresponding to a configuration incorporating MOTIF.

values since the flow structure is identical. This is confirmed for the case of using circular and triangular bund walls. However, the error is significant for square and rectangular walls. This proves that InterFoam does not performs well for these cases, as it was shown in Megdiche et al. (2017). Regarding the reduction in overtopping fractions, COAST permits reductions of 93%, 35%, 10%, and 34% for circular, square, rectangular, and triangular bund walls, respectively.

5.4. Effect of the incorporation of COAST using different heights of fluid

Fig. 18 presents the effect of the incorporation of COAST with

different heights of fluid in the tank. For this set of simulations, the capacity of the bund wall was set to 110%, while varying the height of the fluid and the height of the bund wall accordingly. The various heights of the fluid are 0.6 m, 0.3 m, and 0.12 m corresponding to tall, middle, and squat tanks, respectively. The purpose of these simulations is to investigate the effect of the fluid height on the dynamic pressures and the overtopping fractions while incorporating COAST. The results corresponding to the standard configurations are obtained from the CFD simulations, except for the case of tall tank, as no experimental data was available. It can be noticed that the dynamic pressure increases with an increasing height of the fluid, which implies that taller tanks have more
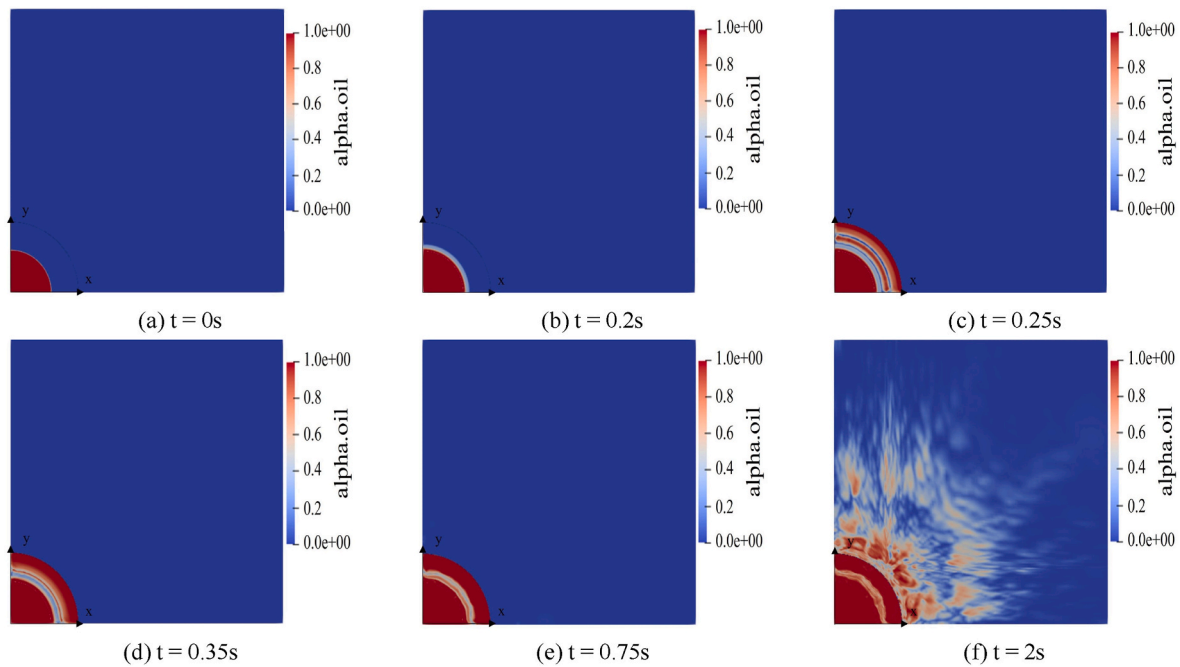
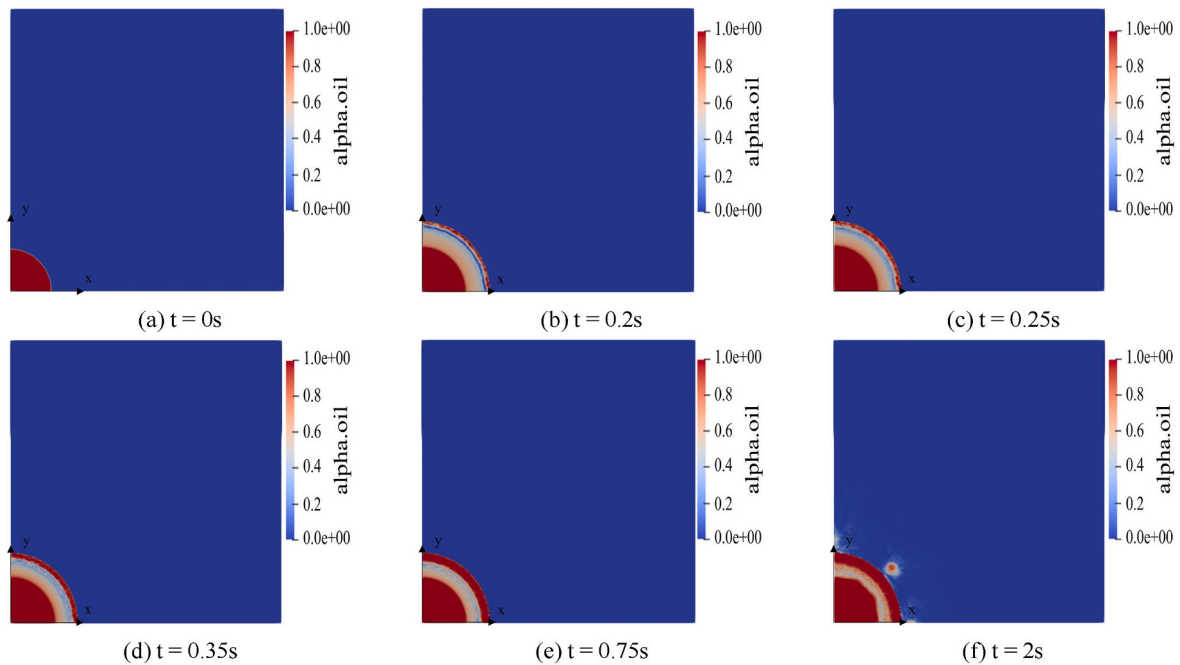**Fig. 14.** A bottom view of the flow corresponding to a configuration incorporating COAST and MOTIF.

Fig. 15. A bottom view of the flow corresponding to a configuration incorporating COAST.

Table 8
Comparison between the various mitigation techniques in terms of dynamic pressures and overtopping fractions.

	MOTIF	COAST	COAST & MOTIF
P (Pa)	5900	5700	7000
Q %	21	1	17

potential energy, hence more kinetic energy after the release, assuming that energy principles are considered. The dynamic pressures obtained from the standard configurations and the configurations incorporating

COAST are close in order of magnitude. Regarding the overtopping fractions, incorporating COAST yields a reduction in overtopping fractions of 93%, 84.52%, and 68.33% for tall, middle, and squat tanks, respectively. This implies that COAST is more effective in the case of tall tanks.

6. Conclusions

In this work, the incorporation of mitigation measures in the primary and secondary containments have been investigated. Their effects on the dynamic pressures and overtopping fractions for the case of catastrophic failure of above-ground storage tanks have been quantified through CFD
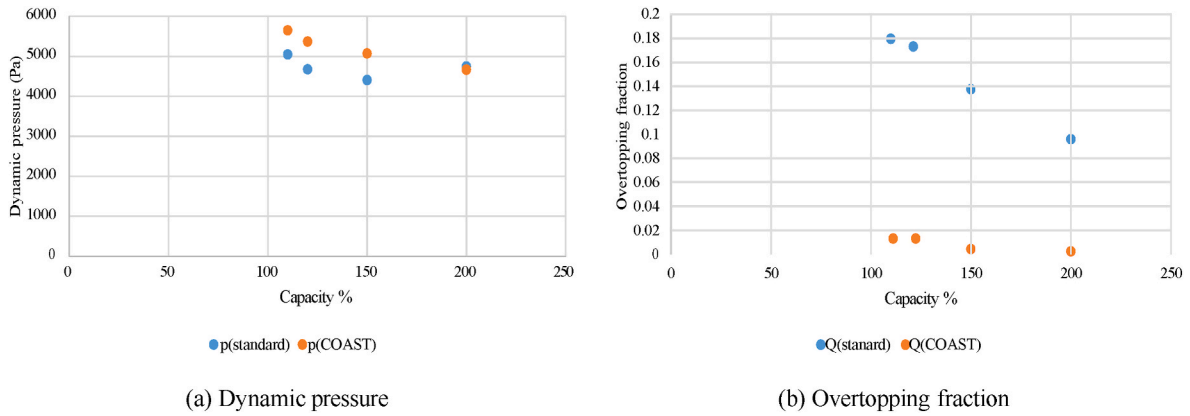
(a) Dynamic pressure

(b) Overtopping fraction

Fig. 16. Effect of COAST with different capacities of the bund wall.

(a) Dynamic pressure

(b) Overtopping fraction
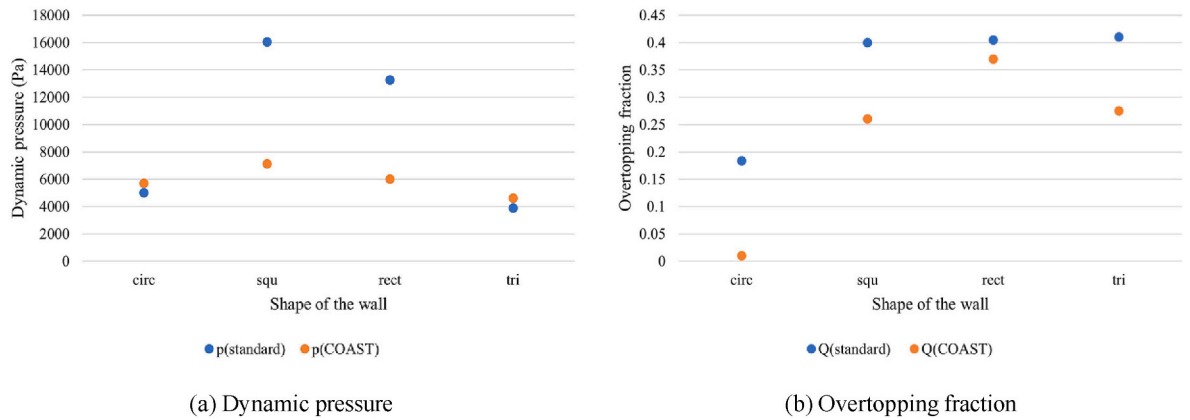
Fig. 17. Effect of COAST with different shapes of the bund wall.

(a) Dynamic pressure
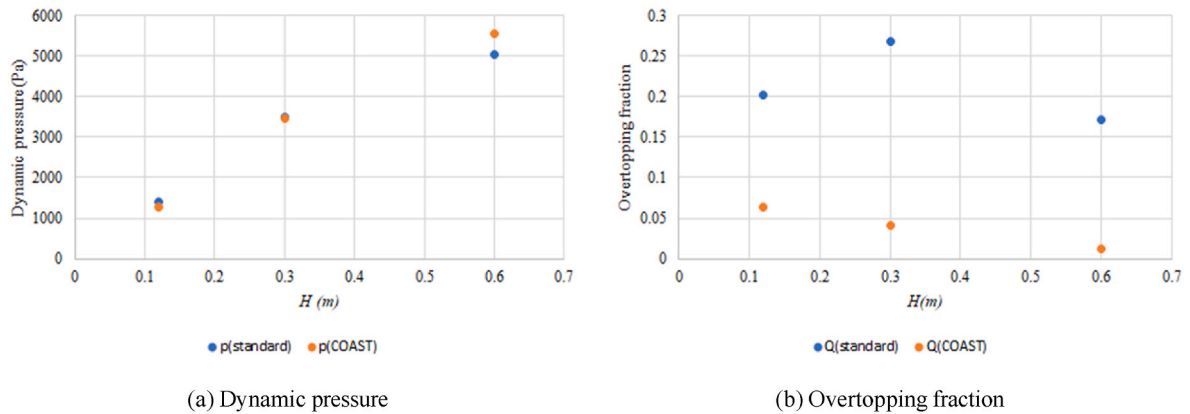
(b) Overtopping fraction

Fig. 18. Effect of COAST with different heights of the fluid.

simulations. For this purpose, the InterFoam solver in OpenFoam software was used. The mitigation measures proposed by Ash (2010) were optimised in this paper. While Ash (2010) proposed to incorporate MOTIF in combination with COAST as they allow significant reduction in the overtopping fractions, CFD simulations conducted in this research showed that for small separation distances, the inclusion of MOTIF modifies the flow structure in such a way that it hits the top of the wall at the first impact. This can increase the risk of failure by increasing the overturning moment. Contrary to that, COAST keeps the same flow structure as the standard cases and permits significant reductions in overtopping quantities. The cost of incorporating COAST is not

significant compared to the cost of the construction of the bund wall if taking into account the savings in the losses. Therefore, COAST is the mitigation measure adopted. The inclination angle of COAST was optimised. COAST with an inclination of 80° achieved a significant reduction in overtopping fractions. Subsequently, further simulations have then been conducted to study the effect of COAST using different capacities, shapes of the bund walls, and heights of the fluid in the tank. Regarding the overtopping fractions, COAST permitted a significant reduction in overtopping fractions for circular bund walls and tall tanks. The highest reduction in overtopping fraction is 98% and corresponds to a tall tank and a bund wall capacity of 200%. The main contribution of

this research is that it constitutes a first step to design a bund wall able to reduce the overtopping fractions and the dynamic pressures. Also, it helps stakeholders to gain insight into the flow behaviour with various mitigation measures implemented and their effect under many parameters.

CRediT authorship contribution statement

Islem Megdiche: Conceptualisation of this study, Methodology, Simulation, Validation, Writing original draft, Writing - review and editing, Visualisation. **William Atherton:** Project administration, Funding acquisition, Conceptualisation, Review and editing. **David Allanson:** Validation, Conceptualisation. **Clare Harris:** Supervision.

Declaration of competing interest

The authors declare that they have no known competing financial interests or personal relationships that could have appeared to influence the work reported in this paper.

Data availability

Data will be made available on request.

Acknowledgement

References

Aftab, S., Mohd Rafie, A., Razak, N., Ahmad, K., 2016. Turbulence model selection for low Reynolds number flows. PLoS One 11, e0153755.

Ash, J.W., 2010. Mitigation of the Catastrophic Failure of the Primary Containment in the Bulk Storage Industry. Ph.D. thesis. Liverpool John Moores University.

Atherton, W., 2008. An Empirical Investigation of Catastrophic and Partial Failures of Bulk Storage Vessels and Subsequent Bund Wall Overtopping and Dynamic Pressures. Ph.D. thesis. Liverpool John Moores University.

Atherton, W., Ash, J., 2007. Review of failures, causes & consequences in the bulk storage industry. In: Proc. 2nd Annu. Liverpool Conf. Built Environment and Natural Environment.

Bredberg, J., 2000. On the Wall Boundary Condition for Turbulence Models. Department of Thermo and fluid dynamics- Chalmers University of Technology. Technical Report.

Cantero, M.I., Balachandar, S., García, M.H., Bock, D., 2008. Turbulent structures in planar gravity currents and their influence on the flow dynamics. J. Geophys. Res. Oceans 113. https://doi.org/10.1029/2007JC004645.

Chang, J.I., Lin, C.C., 2006. A study of storage tank accidents. J. Loss Prev. Process Ind. 19 (1), 51–59.

Deshpande, S.S., Anumolu, L., Trujillo, M.F., 2012. Evaluating the performance of the two-phase flow solver interfoam. Comput. Sci. Discov. 5 (1), 014016.

Gladstone, C., Phillips, J., Sparks, R., 1998. Experiments on bidisperse, constant-volume gravity currents: propagation and sediment deposition. Sedimentology 45, 833–843.

Greenshields, C.J., 2018. OpenFOAM User Guide- Version 6. Technical Report. OpenFOAM Foundation Ltd.

Greenspan, H., Johansson, A.V., 1981. An experimental study of flow over an impounding dike. Stud. Appl. Math. 64, 211–223.

Greenspan, H., Young, R., 1978. Flow over a containment dyke. J. Fluid Mech. 87, 179–192.

Gyenes, Z., Wood, M.H., 2014. Lessons learned from major accidents having significant impact on the environment. In: SYMPOSIUM SERIES.

Heyns, J.A., Oxtoby, O.F., 2014. Modelling surface tension dominated multiphase flows using the vof approach. In: 6th European Conference on Computational Fluid Dynamics.

Huo, J., Luan, X., Gong, Y., Wang, Z., Jiang, J., Zhang, B., 2021. Numerical study of bund overtopping phenomena after a catastrophic tank failure using the axisymmetric approach. Proc. Saf. Environ. Protect. 153, 464–471.

Huo, J., Wang, Z., Luan, X., Jing, M., Hou, S., Jiang, J., Zhang, B., 2022. The cfd modeling of bund overtopping phenomena and prediction of dynamic pressure on the bund. J. Loss Prev. Process Ind. 74, 104653.

Huppert, H.E., Simpson, J.E., 1980. The slumping of gravity currents. J. Fluid Mech. 99, 785–799.

Ivings, M., Webber, D., 2007. Modelling bund overtopping using a shallow water cfd model. J. Loss Prev. Process Ind. 20, 38–44.

Kleefsman, K., Fekken, G., Veldman, A.E., Iwanowski, B., 2004. An improved volume-of-fluid method for wave impact problems. In: The Fourteenth International Offshore and Polar Engineering Conference.

Liu, Q., Chen, Z., Liu, H., Yin, W., Yang, Y., 2017. Cfd simulation of fire dike overtopping from catastrophic ruptured tank at oil depot. J. Loss Prev. Process Ind. 49, 427–436.

Lopes, P., 2013. Free-surface Flow Interface and Air-Entrainment Modelling Using OpenFOAM. Ph.D. thesis. University of Coimbra.

Luan, X., Huo, J., Liu, Y., Jiang, B., 2020. Predictive model of bund overtopping fraction for catastrophic failure of storage tank. Safety Sci. 129, 104801.

Megdiche, I., 2019. Evaluation of the Mechanical Strength of Bund Walls under the Catastrophic Failure of Storage Tanks via Fluid Structure Interaction. Ph.D. thesis. Liverpool John Moores University.

Megdiche, I., Atherton, W., Harris, C., Rothwell, G., Allanson, D., 2017. Computational fluid dynamics modelling of the catastrophic failure of storage tanks. In: Nafmes World Congress 2017.

Menni, Y., Zidani, C., Azzi, A., Benyoucef, B., 2016. Low-Reynolds-number turbulent forced-convection flow over graded baffle plates. J. Renew. Energies 19, 235–250.

Menter, F.R., Kuntz, M., Langtry, R., 2003. Ten years of industrial experience with the sst turbulence model. Turbul. Heat Mass Tran. 4, 625–632.

Nair, S., 2008. Methods of avoiding tank bund overtopping using computational fluid dynamics tool. In: Institution of Chemical Engineers Symposium Series. Institution of Chemical Engineers, p. 479, 1999.

Necker, F., Härtel, C., Kleiser, L., Meiburg, E., 2002. High-resolution simulations of particle-driven gravity currents. Int. J. Multiphase Flow 28, 279–300.

Pettitt, G., Waite, P., 2003. Bund design to prevent overtopping. In: Institution of Chemical Engineers Symposium Series. Institution of Chemical Engineers, pp. 329–340.

Ramajo, D.E., Corzo, S.F., Damian, S.M., Gimenez, J.M., Nigro, N.M., 2018. Numerical investigation of bund overtopping under storage tank failure events. J. Loss Prev. Process Ind. 52, 113–124.

Sahasrabudhe, S.N., Rodriguez-Martinez, V., O'Meara, M., Farkas, B.E., 2017. Density, viscosity, and surface tesnion of five vegetable oils at elevated temperatures: measurement and modeling. Int. J. Food Prop. 20 (2), 1965–1981.

Schmidt, M.S., 2017. Atmospheric tank failures: mechanisms and an unexpected case study. Process Safety Prog.

Simpson, J.E., 1997. Gravity Currents: in the Environment and the Laboratory. Cambridge university press.

Thyer, A., Hirst, I., Jagger, S., 2002. Bund overtopping—the consequence of catastrophic tank failure. J. Loss Prev. Process Ind. 15, 357–363.

Trbojevic, V.M., Slater, D.H., 1989. Tank failure modes and their consequences. Plant/Oper. Prog. 8, 84–87.

Walton, I., 2014. Containment Systems for the Prevention of Pollution. Technical Report. CIRIA.

Webber, D., Ivings, M., 2010. Modelling bund overtopping using shallow water theory. J. Loss Prev. Process Ind. 23, 662–667.

Webber, D., Ivings, M., Maru, W., Thyer, A., 2009. Validation of the Shallow Water Model "Splot" against Experimental Data on Bund overtopping. Health and Safety Executive Research Report RR755.

Zgheib, N., Bonometti, T., Balachandar, S., 2015. Dynamics of non-circular finite-release gravity currents. J. Fluid Mech. 783, 344–378. https://doi.org/10.1017/jfm.2015.580.